Check for updates

Electron density modulation in monolayer MoS$_2$ through the phase transition of a relaxor ferroelectric substrate

David Hernández-Pinilla,[ab] Dennis P. Cachago, [ID][a] Yi An Xia,[a]
Guillermo López-Polín,[ac] Mariola O Ramírez [ID][abc] and Luisa E. Bausá [ID] *[abc]

The integration of transition metal dichalcogenides (TMDs) with ferroelectric substrates is a powerful strategy to modulate their electronic and optical properties. However, the use of relaxor ferroelectrics for this purpose remains unexplored. Here, we demonstrate a reversible photoluminescence (PL) and charge density modulation of monolayer MoS$_2$ on a Sr$_{0.61}$Ba$_{0.39}$Nb$_2$O$_6$ (SBN) substrate, a prototypical relaxor ferroelectric. The smearing of the phase transition in SBN enables continuous tuning of MoS$_2$ electronic properties over a broad temperature range (30–90 °C). A pronounced PL enhancement occurs as the substrate transitions from ferroelectric to paraelectric phase due to the vanishing spontaneous polarization (P_S) and the consequent change in charge balance at the MoS$_2$/SBN interface. Moreover, thermal hysteresis in the electron density modulation is observed during heating and cooling cycles. These findings highlight the potential of relaxor ferroelectrics as reconfigurable platforms for electron doping and light-emission control in 2D materials, opening avenues for temperature-responsive optoelectronic and nanophotonic applications.

New concepts

This work introduces the use of relaxor ferroelectrics with a diffuse phase transition as a novel and underexplored platform for electrostatic modulation of 2D semiconductors. While ferroelectric substrates have been widely employed to achieve nonvolatile control of charge doping in 2D materials, relaxor ferroelectrics had not been considered in this context. We demonstrate that the smooth ferroelectric to paraelectric transition of the relaxor substrate enables continuous, reversible, and purely thermal tuning of the optoelectronic properties of monolayer MoS$_2$, without requiring electrical contacts or external gating. This concept departs from existing approaches that rely on abrupt switching or the application of external fields, providing instead a gradual and contactless control mechanism. The coupling between the environmental sensitivity of 2D materials and the progressive polarization changes of relaxor ferroelectrics offers a new strategy for achieving wide-range and hysteretic modulation of charge density and photoluminescence. This framework opens new opportunities for designing temperature-responsive, reconfigurable systems and optoelectronic components, including artificial synapses and memory devices, where smooth and reversible tuning is essential.

Introduction

Transition metal dichalcogenides (TMDs), such as MoS$_2$, have attracted significant attention due to their exceptional characteristics, including high carrier mobility, tunable band gaps, and light–matter interaction, which make them ideal for applications in photodetectors, transistors, and energy storage.[1–4] As is well known, their properties can be modulated by external stimuli, making them highly versatile for emerging technologies.[5–8] In particular, controlling electron doping in TMDs is crucial for developing tunable switching devices, and different methods such as chemical doping, electrostatic gating, strain, and light fields have been employed.[9–11]

Recently, the use of ferroelectrics as active substrates has emerged as an effective strategy to control the properties of monolayer TMDs (1L-TMDs),[12,13] avoiding complex fabrication that hinders device integration. Various 2D/ferroelectric systems have been explored for applications in memories[14] and optoelectronic devices.[15] A prominent example is lithium niobate (LiNbO$_3$), which provides a versatile platform for tuning the electronic properties of 2D materials.[16] Previous works on 2D/LiNbO$_3$ heterostructures have demonstrated domain-dependent electrostatic doping,[17–19] and polarization-dependent photodoping.[20] More recently, pyroelectric effect has been shown to influence electronic doping, as revealed through optical and transport measurements.[21,22]

In addition to LiNbO$_3$, a variety of other ferroelectrics have been used as gate substrates for 2D materials, including BiFeO$_3$ and PZT for dielectric memories[14,23,24] and BaTiO$_3$ as a ferroelectric dielectric for single-layer MoS$_2$ field-effect devices.[25] All these materials exhibit an abrupt phase transition that

[a] Dept. Física de Materiales, Universidad Autónoma de Madrid, Spain

[b] Instituto de Materiales Nicolás Cabrera (INC), Universidad Autónoma de Madrid, Spain

[c] Condensed Matter Physics Center (IFIMAC), Universidad Autónoma de Madrid, Spain

occurs well above room temperature. In this context, ferroelectric substrates with lower and more accessible transition temperatures are particularly appealing, as they allow the study of substrate-induced modulation of optical and electrical properties without risking deterioration of the 2D layer.

Moreover, the integration of 2D materials with relaxor ferroelectrics has yet to be explored. In these systems, the Curie temperature (T_C) is not sharply defined. Instead, they exhibit a gradual transition from the ferroelectric to the paraelectric phase. This feature enables the study of various physical phenomena across the phase transition, as the material evolves from the ferroelectric to the paraelectric phase or *vice versa*,[26–29] where pronounced changes of the relevant physical magnitudes are expected.

In this work, an $Sr_xBa_{1-x}Nb_2O_6$ crystal (hereafter SBN) is used as an active substrate for a MoS_2 monolayer (1L-MoS_2). This crystal belongs to the attractive class of relaxor ferroelectrics[30] and, additionally, presents remarkable properties such as large pyroelectric and electro-optical coefficients, as well as favorable photorefractive and acousto-optic characteristics,[31] potentially useful for integrated devices. Indeed, SBN has been proposed for a wide range of applications in photonics, data storage, or switching.[32–35]

The structure of SBN exhibits notable cationic disorder, with ion distribution occurring in a disordered manner across different coordination environments.[36,37] This underlies the smearing of the phase transition, which occurs over a relatively broad temperature range.[38] Additionally, the structural cation disorder and compositional fluctuations lead to local symmetry distortions, so that SBN crystals typically contain randomly embedded inclusions of small, spontaneously polarized regions. In fact, as previously reported, SBN exhibits a disordered distribution of anti-parallel, needle-like ferroelectric domains, with the longest dimension aligned along the optical c-axis.[39,40]

In our work, the SBN crystal used as a substrate corresponds to a composition of $x = 0.61$, which exhibits a T_C around 70 °C.[29] This relatively low T_C value ensures the monolayer is not exposed to high temperatures that could cause degradation, which typically occurs around 250 °C for 1L-MoS_2.[41] As a result, reliable measurements of its optical and electronic properties can be performed during the heating/cooling process. Indeed, this moderate transition temperature is particularly advantageous for the development of reconfigurable or thermally driven devices, where operation near room temperature is essential.

The objective in this work is to investigate the influence of the ferroelectric to paraelectric transition on the optical and electronic properties of 1L-MoS_2 that has been transferred onto the polar surface of an SBN substrate. To this end, we study the evolution of the photoluminescence (PL) of 1L-MoS_2 around T_C of SBN, within the 30–90 °C range in which the relaxor phase transition takes place. As the substrate undergoes from the ferroelectric to the paraelectric phase, a significant enhancement in the 1L-MoS_2 emission intensity is observed. This enhanced emission is attributed to the vanishing of P_S as the substrate transitions to the paraelectric phase, which alters the polarization/screening-charge balance at the 1L-MoS_2/SBN interface, thereby modulating the carrier density in the 1L-MoS_2.

The work demonstrates the reversibility of the modulation of the PL and electron doping through the substrate phase transition while featuring a hysteretic behavior. This highlights the reconfigurable ability of the substrate to induce switchable functionality through its interaction with the 2D material. The findings show a robust strategy for electrostatic carrier modulation in 1L-TMDs, demonstrating the potential for temperature-responsive optoelectronic devices that do not require external electric fields.

Experimental

Sample preparation

A single congruent SBN ($x = 0.61$) crystal was grown by the Czochralski technique. The crystal contained a small amount of Yb^{3+} (0.6 at% referred to Nb^{5+} atoms). Plate samples were cut with the c-axis oriented perpendicular to the main face and then polished to achieve optical quality. Optical microscopy images were obtained in reflection mode using an Olympus BX51 microscope equipped with an Olympus DP72 camera. MoS_2 flakes were mechanically exfoliated from a bulk crystal, deposited onto a polydimethylsiloxane sheet, and subsequently deterministically transferred[42] at room temperature onto the main face of the SBN substrate. The monolayer character of the transferred MoS_2 flake was confirmed by differential microreflectance spectroscopy. An SiO_2 glass substrate was also used as a reference for the thermal evolution of the PL in 1L-MoS_2. To reveal the presence of the domain structure in the SBN substrate, chemical etching was performed using a 2:1 solution of HNO_3:HF at room temperature for 4 hours. We note, however, that in all experiments presented in this work, 1L-MoS_2 was transferred onto a polished, unetched SBN surface where no etch pits were observed.

Optical measurements

PL measurements were performed using a custom laser scanning confocal microscope (Olympus BX41), equipped with a motorized XY stage. An Ar^+ laser was used as excitation light source. Excitation power was fixed at 13.2 kW cm^{-2} to avoid photodoping effects[20] and over-heating the sample. For second harmonic generation (SHG) experiments, the same confocal microscope system was employed. A femtosecond-pulsed Ti:sapphire laser (Spectra Physics Model 177-Series), operating at a wavelength of 800 nm, was used as the fundamental excitation source for SHG. In both types of optical measurements, the incident beam was focused on the sample using a 50× objective lens (NA = 0.35). The emission signals were collected in a backscattering geometry through the same objective by an optical fiber coupled to a Horiba iHR 550 monochromator. A Peltier-cooled Horiba Synapse CCD was used for the detection.

To induce phase transitions during the PL experiments, the 1L-MoS_2/SBN sample was mounted on a heating platform

(Linkam PE120) controlled by a T96 Peltier linkPad. Temperature was measured by means of chromel-alumel thermocouple place on the lateral face of the sample. Each emission spectrum was recorded once a steady-state temperature (equilibrium) was reached.

Results and discussion

Fig. 1a shows a schematic representation of the system used in this work. It consists of a 1L-MoS$_2$ transferred onto the polar surface of a SBN relaxor ferroelectric crystal. Details on the sample preparation are provided in the Methods section.

A prior characterization of the SBN substrate before MoS$_2$ deposition is of particular interest. On one hand, the characterization of the domain structures has been performed by optical microscopy. Fig. 1b shows an optical image of the c-

Fig. 1 (a) Schematics of the 1L-MoS$_2$ transferred on a SBN ferroelectric substrate. (b) Optical image of the ferroelectric domain distribution on the ab plane of the SBN crystal. Scale bar: 1 μm. (c) Evolution of the SHG intensity of SBN as a function of temperature around the relaxor ferroelectric to paraelectric phase transition. Evolution of the PL spectra of 1L-MoS$_2$ with increasing temperature on a (d) SiO$_2$ and a (e) SBN substrate. (f) PL intensity evolution of 1L-MoS$_2$ on SiO$_2$ (blue) and SBN (red) as the temperature increases. The lines are guides to the eyes.

surface of the SBN crystal revealing a random distribution of ferroelectric domains in the ab plane after selective chemical etching. The observed distribution is consistent with previous reports, which described needle-like ferroelectric domains with a quasi-square cross-section,[26,43] with their longest dimension parallel to the optical c-axis. In our case, the average domain diameter is approximately 500 nm.

On the other hand, determining the phase transition temperature is also crucial in the context of this work. To that aim, non-invasive optical measurements have been used. In particular, SHG has been employed, since investigating the evolution of quadratic optical nonlinear phenomena provides a reliable and direct means to track symmetry changes in the crystal. Fig. 1c illustrates the evolution of the SHG signal of the SBN substrate as a function of temperature. At room temperature, the crystal is in its ferroelectric phase characterized by the noncentrosymmetric tetragonal space group P4bm, which allows quadratic nonlinear optical processes such as SHG. As the temperature increases, a noticeable change in the SHG intensity is observed, due to the transition towards the centrosymmetric paraelectric phase, where the quadratic nonlinear optical effects vanish. Namely, the SHG signal gradually decreases with increasing temperature in the 30–70 °C range, according to the relaxor character of SBN, until it reaches a value of nearly zero at around 73 °C, which we identify as the T_C of our substrate. This value is similar to those previously reported for SBN crystals with the same stoichiometry ($x = 0.61$).[29,38]

Once the domain structure and the relaxor ferroelectric behavior have been established, 1L-MoS$_2$ was transferred onto a polished, unetched SBN surface. We have analyzed the PL of 1L-MoS$_2$ on the SBN substrate as a function of temperature around the phase transition. To isolate the effects of the phase transition from those of temperature-induced changes in the emission rate, the evolution of the PL of 1L-MoS$_2$ on SBN is compared to that on SiO$_2$, a system that does not undergo a phase transition. The temperature is varied from 30 °C to 90 °C, and PL spectra is measured at intervals of 5–10 °C. For clarity, only selected spectra at some specific temperatures are shown.

Fig. 1d and e present the emission spectra of both systems in the region of the A-exciton, measured under the same conditions as the temperature increases. The most significant difference between the two series of spectra lies in their intensity. While the PL of 1L-MoS$_2$/SiO$_2$ shows no significant changes in intensity with increasing temperature, the 1L-MoS$_2$/ SBN system exhibits remarkable enhancement in emission, with the intensity at 90 °C reaching nearly twice that at room temperature. Fig. 1f shows the comparison of PL intensity evolution of 1L-MoS$_2$ on SiO$_2$ and on SBN as the temperature increases. The difference in the PL intensity behavior of 1L-MoS$_2$ on SBN compared to SiO$_2$ is attributed to the SBN relaxor ferroelectric to paraelectric phase transition. In fact, once the SBN substrate has reached the paraelectric phase, where the spontaneous polarization is zero (non-polar phase), the PL intensity does not exhibit significant changes within the studied temperature range, consistent with the observations for
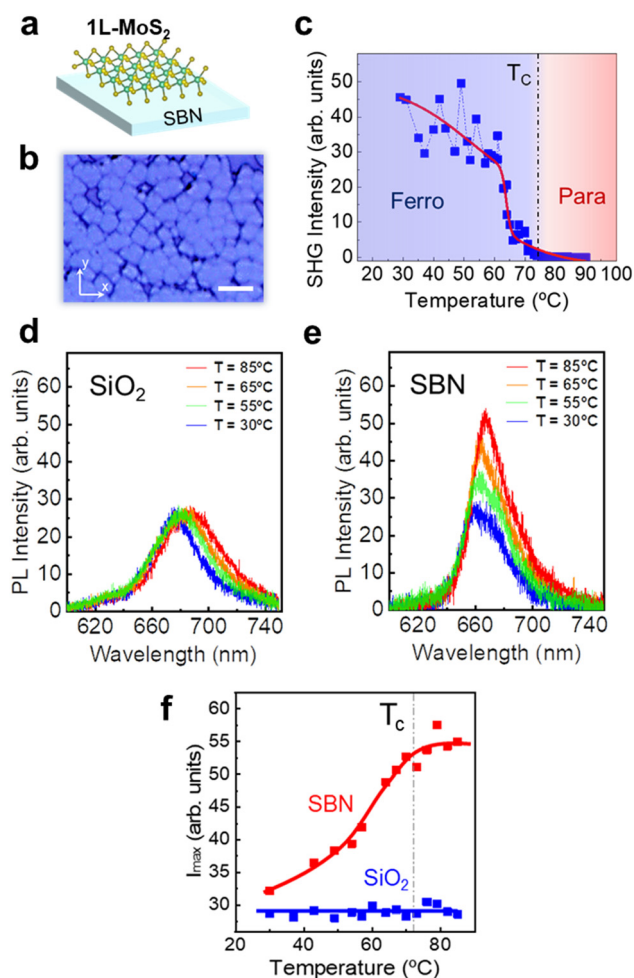
1L-MoS$_2$ on a non-polar SiO$_2$ substrate. The possibility of PL enhancement in MoS$_2$ using a substrate that undergoes an insulator-to-metal phase transition has been reported. However, the observed enhancement is attributed to constructive optical interference when the substrate becomes metallic.[44]

A more detailed analysis of the spectra reveals further differences between both types of systems. In the PL spectra of Fig. 1d, the emission from 1L-MoS$_2$/SiO$_2$ can be primarily attributed to negative trions (*i.e.*, two electrons and one hole), with a band peaking at approximately 675 nm at room temperature,[45] which redshifts as the temperature increases due to thermal-induced effects.[46] The predominantly trionic character of the emission is consistent with the intrinsic n-type doping of MoS$_2$ layers and the prominent electron doping provided by the SiO$_2$ substrate,[47] which persists across the entire temperature range studied. In contrast, as observed in Fig. 1e, the PL spectra of 1L-MoS$_2$/SBN reveal emission from two types of quasiparticles: excitons (*i.e.* electron–hole pairs) and trions, with peaks at around 658 nm and 675 nm, respectively, at room temperature. The thermal evolution of these spectra also exhibits a redshift. However, in contrast to the SiO$_2$ substrate, a significant intensity enhancement is observed at the highest temperatures. Moreover, as the temperature increases, a clear conversion of trion into neutral exciton emission occurs, as will be shown in further detail below.

The observed differences can be attributed to the substrate effect. Specifically, the different excitonic contribution in the room temperature spectrum of 1L-MoS$_2$/SBN with respect to that of 1L-MoS$_2$/SiO$_2$, can be linked to the effect of the ferroelectric substrate, which induce a modulation of the electron density in agreement with previous studies.[20]

To clearly visualize the modification of the 1L-MoS$_2$ PL occurring during the phase transition, we compare the spectra taken at both ends of the temperature range, in the ferroelectric and paraelectric phases, as shown in Fig. 2a. There, the increase in PL intensity as the substrate transitions from the ferroelectric to the paraelectric phase is readily observed. These spectra have been deconvoluted into their exciton and trion contributions, using Lorentzian bands (Fig. 2b). This analysis reveals that the increased emission intensity in the paraelectric phase is linked to the enhancement of excitonic emission, while the trion emission remains essentially constant. The evolution of the exciton-to-trion intensity ratio across the entire temperature range is shown in Fig. 2c. As observed, this ratio increases monotonically with increasing temperature in the 30–70 °C range, indicating a gradual variation of the electron density of the monolayer up to the T_C, after which the exciton-to-trion intensity ratio remains practically constant. This result correlates well with the relaxor phase transition of the SBN substrate, which, according to Fig. 1c, occurs around 73 °C.

The observed variations in 1L-MoS$_2$/SBN PL can be related to changes in the electronic density (n_e), which can be estimated from the spectral weight ratio of trions to excitons. Based on the mass action law, which describes the equilibrium between excitons, trions, and free electrons, n_e can be determined from the PL spectra without requiring electrical measurements, as follows:[45]

$$\frac{I_{X^-}}{I_X} = \frac{n_e}{\eta_r C(T)} \quad (1)$$

where I_{X^-} and I_X represent the intensity contribution of trions and excitons to the spectra, respectively. η_r denotes the relative quantum yield of the exciton and the trion ($\eta_r = \eta_X/\eta_{X^-}$), while $C(T)$ is a function of temperature, which is given by

$$C(T) = \left(\frac{4m_X m_e}{\pi \hbar^2 m_{X^-}}\right) \cdot k_B T \cdot e^{-E_b/k_B T} \quad (2)$$

Here, m_X, m_{X^-} and m_e refer to the effective masses of excitons, trions and electrons, respectively, with values of $m_X = 0.8m_0$, $m_{X^-} = 1.15m_0$ and $m_e = 0.35m_0$ for 1L-MoS$_2$,[22] where m_0 is the
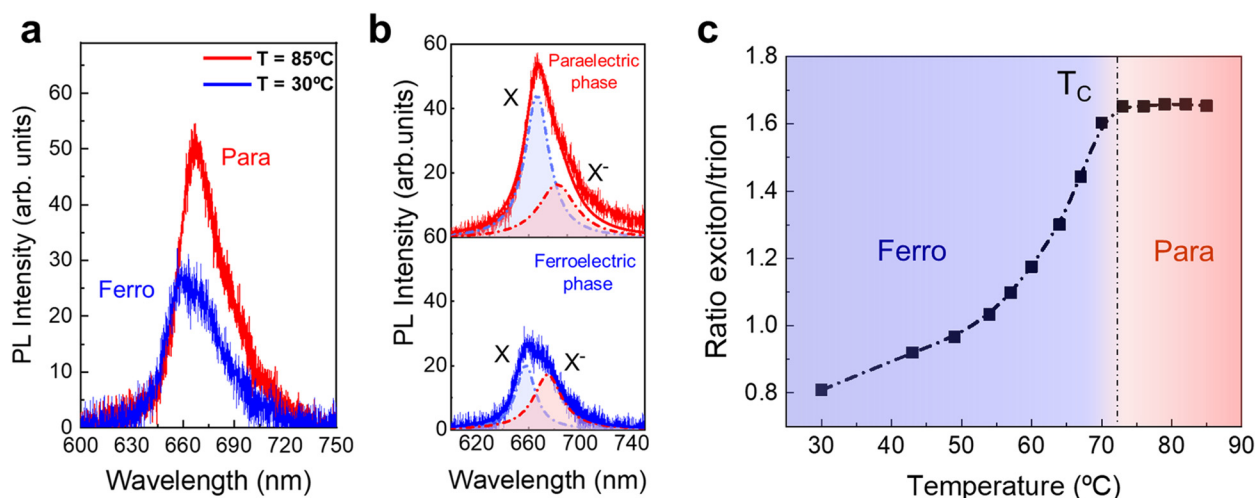

Fig. 2 (a) Comparison of the emission spectra of the 1L-MoS$_2$ in the ferroelectric and paraelectric phases of the SBN substrate. (b) Deconvoluted PL spectra of 1L-MoS$_2$ showing the exciton and trion contributions in the ferroelectric and paraelectric phases of the SBN substrate. The labels X and X$^-$ refer to exciton and trion, respectively. (c) Evolution of the exciton-to-trion intensity ratio of 1L-MoS$_2$ with increasing temperature across the ferroelectric to paraelectric transition of SBN. The line is a guide to the eyes.

free electron mass. The trion binding energy is $E_b \simeq 20$ meV.[48] At 300 K, $C(T)$ takes a value of 4.86×10^{12} cm^{-2}. The radiative emission rate of the exciton is significantly higher than that of the trion, and η_r has been approximated to 20/3.[45] This value has been kept fixed throughout the analysed temperature range.

Fig. 3a shows the electron density (in μC cm^{-2}) in 1L-MoS$_2$ as a function of increasing temperature within the phase transition range of the SBN substrate. Around room temperature, the electron density reaches a value of around 14 μC cm^{-2} (9×10^{13} e$^-$ cm^{-2}), which gradually decreases through the phase transition. For higher temperatures, the charge density remains practically constant in the studied range, at a value of approximately $\Delta\sigma = 8$ μC cm^{-2}. The observed electron density evolution in 1L-MoS$_2$ can be associated with the gradual disappearance of P_S in the SBN substrate as it undergoes the relaxor ferroelectric to paraelectric phase transition. As a consequence, throughout the phase transition, a reduction in the polarization charge of the substrate occurs, modifying the charge balance at the 1L-MoS$_2$/SBN interface, and thus, the electron doping of the monolayer. In contrast, in the paraelectric phase, P_S is zero, and the surface charge of the substrate is no longer altered, thereby maintaining the charge at the 1L-MoS$_2$/SBN interface mostly constant.

However, it is important to consider that the SBN substrate exhibits a ferroelectric domain distribution that results in regions with oppositely oriented polarization. In this scenario, as temperature increases, 1L-MoS$_2$ is expected to undergo the same charge density change (Δn_e) on SBN regions with opposite polarization orientations, but with the corresponding opposite sign. Fig. 3b sketches the variation in the interfacial screening and polarization charge associated with the disappearance of P_S on both domain orientations (P_{up} and P_{down}). The net electron doping of 1L-MoS$_2$ is not represented. As the temperature increases, the decrease in P_S reduces the positive or negative polarization charge of the substrate depending on the domain orientation, leading to a charge imbalance at the 1L-MoS$_2$/SBN interface. As a result, the electron doping is

modulated, increasing the electron density on the positive domains and decreasing it on the negative ones.

A point that should be addressed concerns the ferroelectric domain distribution of the SBN substrate. The obtained PL contain the contribution of 1L-MoS$_2$ from both type of domains with oppositely oriented polarizations (P_{up} and P_{down}). In fact, the recorded spectra are an average of the expected emissions from 1L-MoS$_2$ on each type of domain orientation. This averaging effect arises from the domain size in SBN (average of 500 nm) and the spot size of our experiments (~ 2 μm), which prevents the detection of contributions of MoS$_2$ emission on isolated single domains. In addition, it should be noted that, while exciton PL intensity is highly sensitive to variations in electron doping, the PL intensity of trions exhibits an almost negligible dependence on electron doping.[49] Therefore, although 1L-MoS$_2$ on P_{up} domains experiences an increase in negative doping, the expected increase in PL trion from P_{up} is minimal. Meanwhile, the observed PL exciton enhancement, which should originate on the P_{down} domains, is also affected by the decreasing contribution from the P_{up} domain. Since both domains contribute simultaneously to the PL, the resulting signal is averaged, masking the intrinsic I_{X^-}/I_X ratio on each domain and, consequently, the full extent of their respective doping variations. As a result, the net charge variation in 1L-MoS$_2$ extracted from our PL measurements is smaller than changes reported for P_S in close SBN compositions from electrical measurements in single-domain crystals (which range from 15 to 20 μC cm^{-2}).[50]

Similar $\Delta\sigma$ values have been obtained for a different 1L-MoS$_2$ with higher initial electron doping. This highlights that the electron doping modulation is independent of the starting doping, being determined by the variation in P_S. As a figure of merit, the evolution of the magnitude characterizing the electron modulation, $\Delta\sigma$, is shown as a function of temperature for a full thermal cycle: heating up to T_C followed by cooling down to room temperature (see Fig. 4). Upon increasing the temperature, the gradual decrease in $\Delta\sigma$ is observed until it becomes zero at approximately 73 °C. On the other hand, the values corresponding to the temperature decrease show that the system returns to its initial state upon reaching room temperature. This result demonstrates the possibility of a reversible modulation of the optical and electronic properties of the 2D material, highlighting the substrate ability to act as a reconfigurable platform.

In addition, the most notable observation is the presence of thermal hysteresis in the modulation of electron density. That is, the transition temperature upon heating differs from that upon cooling, leading to a shift in the observed transition temperature. This hysteretic behavior is inherent to SBN, as demonstrated in a variety of properties analyzed in this crystal along the phase transition[28,29,51] and has been related to defects and cationic disorder in the lattice that introduces local compositional disorder as well as to domain reconfiguration and pinning. In our case, the hysteresis of SBN confers bistability to the electronic and optical properties of the 2D material.
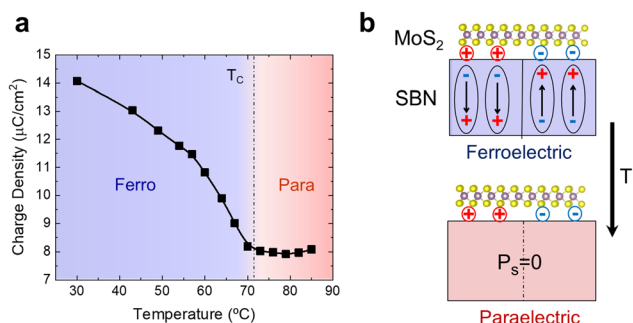
Fig. 3 (a) Evolution of electron doping in 1L-MoS$_2$ as temperature increases across the phase transition of the SBN substrate. (b) Schematics of the cross section of the 1L-MoS$_2$/SBN interface. Modification of the screening/polarization charge balance at the 1L-MoS$_2$ interface as the temperature increases. The net electron doping of 1L-MoS$_2$ is not represented. Top: system in the ferroelectric phase with arrows representing spontaneous polarization. Bottom: system in the paraelectric phase after heating. Screening charges are represented by circles.
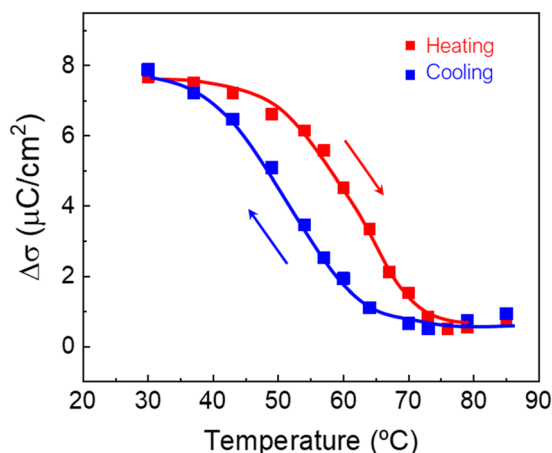
Fig. 4 Temperature dependence of the net change in electron density of 1L-MoS$_2$ exhibiting hysteresis between heating (red squares) and cooling (blue squares) processes around the phase transition of the SBN substrate. Solid lines are a guide to the eye.

In order to analyze whether other spectroscopic parameters of the 1L-MoS$_2$ PL are affected by the phase transition, we have studied the evolution of the spectral position and full width at half maximum (FWHM) of the excitonic band as a function of temperature for heating and cooling.

Fig. 5a shows the evolution of the exciton energy in the 30–90 °C range upon heating and cooling. As observed, no changes or singularities that can be associated with the phase transition of the substrate are detected, nor is there any evidence of a hysteresis cycle. Moreover, the energy of the exciton decreases with increasing temperature, following the expected redshift that can be well described by a standard hyperbolic cotangent relation:[52]

$$E_G(T) = E_G(0) - S\langle \hbar w \rangle \left\{ \coth\left[\frac{\langle \hbar w \rangle}{2k_B T}\right] - 1 \right\} \quad (3)$$

which characterizes the temperature dependence of the optical band gap energy, $E_G(T)$, with respect to its value at 0 K, $E_G(0)$. S is the electron–phonon coupling constant, k_B is Boltzmann's constant and $\langle \hbar w \rangle$ is the average energy of the relevant phonons, taken as 24 meV.[52] The solid line in Fig. 5a corresponds to the fit of the experimental data to eqn (3) with $E_G(0) = 1.97 \pm 0.01$ eV and $S = 2.94 \pm 0.20$, consistent with previously reported values for MoS$_2$.[45,53]

The evolution of the FWHM is displayed on Fig. 5b. Again, no abrupt changes or hysteresis are detected in this parameter as the SBN substrate undergoes the ferroelectric to paraelectric phase transition and the evolution of the bandwidth with increasing temperature follows a phonon-induced broadening that can be approximated by the phenomenological expression:[53]

$$\gamma = \gamma_0 + c_1 T + \frac{c_2}{e^{\left(\frac{\langle \hbar w \rangle}{k_B T}\right)} - 1} \quad (4)$$

where γ_0 and c_1 corresponds to the linear increase due to acoustic phonons, c_2 describes the strength of the phonon coupling and $\langle \hbar w \rangle$ is the average phonon energy. The fitting values of γ_0 and $\langle \hbar w \rangle$ have been taken as $\gamma_0 = 4$ meV and $\langle \hbar w \rangle = 24$ meV.[53] The curve in Fig. 5b corresponds to the fit of the experimental data to eqn (4) with $c_1 = 0.073 \pm 0.015$ meV and $c_2 = 45 \pm 7$ meV, in agreement with previous works.[53]

The energy positions and linewidths that characterize the emitting species follow the expected behavior for 1L-MoS$_2$ as a function of temperature, with no discontinuities or thermal hysteresis. This indicates that the 2D material itself is not influenced by the phase transition of the substrate beyond the changes in electronic doping, which are reflected in the relative emission intensities of the quasiparticles. Therefore, for potential applications, the modulation in device performance primarily would arise from changes in electronic doping induced by the substrate phase change, rather than from structural modifications of the 2D layer. This would allow reliable and
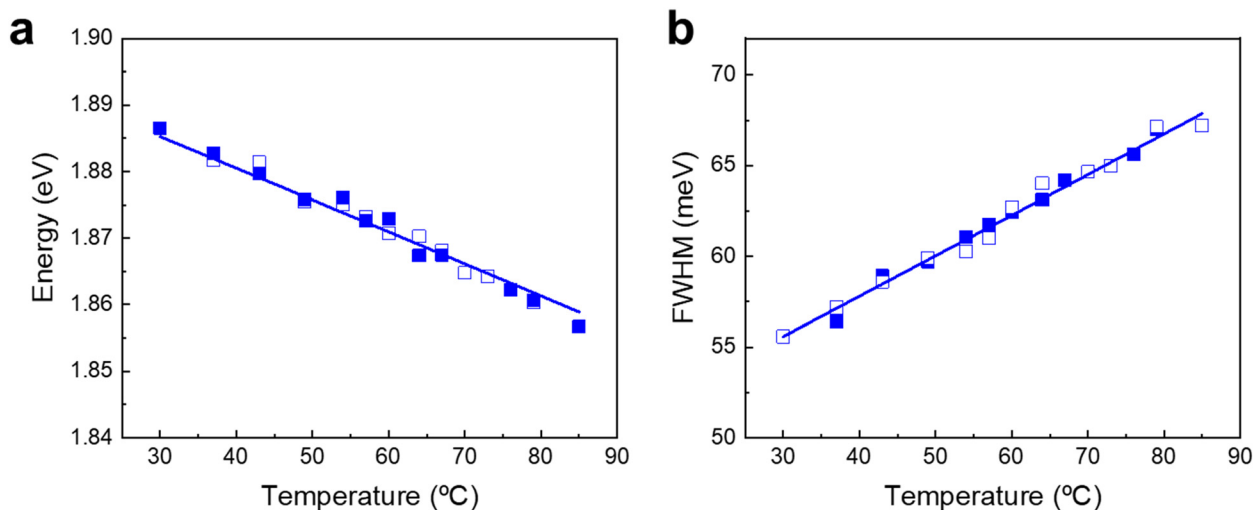

Fig. 5 (a) Spectral positions of the exciton in 1L-MoS$_2$/SBN during heating (full squares) and cooling (open squares). The data are fitted to the semi-empirical O'Donnell–Chen equation (ref. 51). (b) FWHM of the exciton band upon heating (full squares) and cooling (open squares). The solid line represents a fit to eqn (4).

reversible tuning of the electronic and optical properties of the 2D material through temperature control of the substrate phase, without risking degradation or irreversible changes to the 2D material itself. Such stability is highly desirable for devices like sensors, optoelectronic modulators, or memory elements, where controllable and repeatable switching of properties is essential. Moreover, it opens the possibility of designing reconfigurable devices that exploit the substrate phase transition to dynamically and reversibly modulate doping and, consequently, device response.

Conclusions

In this work, we have demonstrated the reversible modulation of the PL and charge density of 1L-MoS_2 by exploiting the ferroelectric to paraelectric phase transition of a relaxor ferroelectric SBN substrate. This transition enables smooth and tunable control over the electronic properties of MoS_2 within a broad temperature range (30–90 °C).

The hysteretic behavior observed in both the PL intensity and doping concentration of 1L-MoS_2 reflects the intrinsic ferroelectric-like response of the SBN substrate across its phase transition. This behavior can be harnessed in applications that benefit from non-volatile, history-dependent states, such as memory storage or artificial synapses, where reversible and temperature-tunable characteristics are essential.

Overall, our results highlight the potential of relaxor ferroelectrics as versatile platforms for smooth, electrostatic modulation of charge in 2D materials, without requiring external fields or mechanical stress. This approach offers a promising route toward reconfigurable optoelectronic and nanophotonic devices integrating 2D-ferroelectric hybrid systems.

Data availability

The data that support the findings of this study are available from the corresponding author upon reasonable request.

Conflicts of interest

There are no conflicts to declare.

Acknowledgements

References

1 S. Manzeli, D. Ovchinnikov, D. Pasquier, O. V. Yazyev and A. Kis, *Nat. Rev. Mater.*, 2017, **2**, 17033.
2 A. Ahmed, M. Z. Iqbal, A. Dahshan, S. Aftab, H. H. Hegazy and E. S. Yousef, *Nanoscale*, 2024, **16**, 2097.
3 J. Chen, M. Y. Sun, Z. H. Wang, Z. Zhang, K. Zhang, S. Wang, Y. Zhang, X. Wu, T. L. Ren, H. Liu and L. Han, *Nanomicro Lett.*, 2024, **16**, 264.
4 S. Kamila, M. Kandasamy, B. Chakraborty and B. K. Jena, *J. Energy Storage*, 2024, **89**, 111614.
5 K. C. Kwon, J. H. Baek, K. Hong, S. Y. Kim and H. W. Jang, *Nanomicro Lett.*, 2022, **14**, 58.
6 X. Tang, Q. Hao, X. Hou, L. Lan, M. Li, L. Yao, X. Zhao, Z. Ni, X. Fan and T. Qiu, *Adv. Mater.*, 2024, **36**, 2312348.
7 D. Thureja, A. Imamoglu, T. Smoleński, I. Amelio, A. Popert, T. Chervy, X. Lu, S. Liu, K. Barmak, K. Watanabe, T. Taniguchi, D. J. Norris, M. Kronera and P. A. Murthy, *Nature*, 2022, **606**, 298.
8 G. Kim, B. Huet, C. E. Stevens, K. Jo, J. Y. Tsai, S. Bachu, M. Leger, S. Song, M. Rahaman, K. Y. Ma, N. R. Glavin, H. S. Shin, N. Alem, Q. Yan, J. R. Hendrickson, J. M. Redwing and D. Jariwala, *Nat. Commun.*, 2024, **15**, 6361.
9 J. Kim, M. Jung, D. U. Lim, D. Rhee, S. H. Jung, H. K. Cho, H. K. Kim, J. H. Cho and J. Kang, *Nano Lett.*, 2022, **22**(2), 570.
10 A. Castellanos-Gomez, R. Roldán, E. Cappelluti, M. Buscema, F. Guinea, H. S. J. van der Zant and G. A. Steele, *Nano Lett.*, 2013, **13**(11), 5361.
11 B. W. H. Baugher, H. O. H. Churchill, Y. Yafang and P. Jarillo-Herrero, *Nat. Nanotechnol.*, 2014, **9**, 262.
12 P. G. Pacchioni, *Nat. Rev. Mater.*, 2023, **8**, 644.
13 S. Kamaei, X. Liu, A. Saeidi, Y. Wei, C. Gastaldi, J. Brugger and A. M. Ionescu, *Nat. Electron.*, 2023, **6**, 658.
14 A. Lipatov, P. Sharma, A. Gruverman and A. Sinitskii, *ACS Nano*, 2015, **9**, 8089.
15 Y. Sun, G. Niu, W. Ren, X. Meng, J. Zhao, W. Luo, Z. G. Ye and Y. H. Xie, *ACS Nano*, 2021, **15**, 10982.
16 X. Liang, H. Guan, K. Luo, Z. He, A. Liang, W. Zhang, Q. Lin, Z. Yang, H. Zhang, C. Xu, H. Xie, F. Liu, F. Ma, T. Yang and H. Lu, *Laser Photonics Rev.*, 2013, **17**, 2300286.
17 C. Baeumer, D. Saldana-Greco, J. M. P. Martirez, A. M. Rappe, M. Shim and L. W. Martin, *Nat. Commun.*, 2015, **6**, 6136.
18 B. Wen, Y. Zhu, D. Yudistira, A. Boes, L. Zhang, T. Yidirim, B. Liu, H. Yan, X. Sun, Y. Zhou, Y. Xue, Y. Zhang, L. Fu, A. Mitchell, H. Zhang and Y. Lu, *ACS Nano*, 2019, **13**, 5335.
19 P. Soubelet, J. Klein, J. Wierzbowski, R. Silvioli, F. Sigger, A. V. Stier, K. Gallo and J. J. Finley, *Nano Lett.*, 2021, **2**, 959.
20 M. O Ramirez, J. Fernandez-Tejedor, D. Gallego, J. Fernández-Martinez, P. Molina, D. Hernández-Pinilla, J. Gómez-Herrero, P. Ares and L. E. Bausá, *Adv. Opt. Mater.*, 2024, **12**, 2400624.

21 J. Fernández-Martínez, J. J. Ronquillo, G. López-Polín, H. P. van der Meulen, M. O Ramírez and L. E. Bausá, *Adv. Opt. Mater.*, 2025, 2500891.

22 Y. Mou, Q. Liu, J. Liu, Y. Xia, Z. Guo, W. Song, J. Gu, Z. Xu, W. Wang, H. Guo, W. Shi, J. Shen and C. Zhang, *Nano Lett.*, 2025, **25**(10), 4029.

23 J. W. Chen, S. T. Lo, S. C. Ho, S. S. Wong, T. H. Y. Vu, X. Q. Zhang, Y. D. Liu, Y. Y. Chiou, Y. X. Chen, J. C. Yang, Y. C. Chen, Y. H. Chu, Y. H. Lee, C. J. Chung, T. M. Chen, C. H. Chen and C. L. Wu, *Nat. Commun.*, 2018, **9**, 3143.

24 Q. Liu, S. Cui, R. Bian, E. Pan, G. Cao, W. Li and F. Liu, *ACS Nano*, 2024, **18**(3), 1778.

25 S. Puebla, T. Pucher, V. Rouco, G. Sanchez-Santolino, Y. Xie, V. Zamora, F. A. Cuellar, F. J. Mompean, C. Leon, J. O. Island, M. Garcia-Hernandez, J. Santamaria, C. Munuera and A. Castellanos-Gomez, *Nano Lett.*, 2022, **22**(18), 7457.

26 M. Ayoub, J. Imbrock and C. Denz, *Opt. Mater. Express*, 2017, **7**, 3448.

27 H. Pan, S. Lan, S. Xu, Q. Zhang, H. Yao, Y. Liu, F. Meng, E. J. Guo, L. Gu, D. Yi, X. R. Wang, H. Huang, J. L. MacManus-Driscoll, L. Q. Chen, K. J. Jin, C. W. Nan and Y. H. Lin, *Science*, 2021, **374**, 100.

28 M. O Ramírez, D. Jaque, L. E. Bausá, J. G. Solé and A. A. Kaminskii, *Phys. Rev. Lett.*, 2005, **95**, 267401.

29 M. O Ramírez, L. E. Bausá, A. Speghini, M. Bettinelli, L. I. Ivleva and J. G. Solé, *Phys. Rev. B: Condens. Matter Mater. Phys.*, 2006, **73**, 035119.

30 L. E. Cross, *Ferroelectrics*, 1994, **151**, 305.

31 R. R. Neurgaonkar, W. F. Hall, J. R. Oliver, W. H. Ho and W. K. Cory, *Ferroelectrics*, 1988, **87**, 167.

32 R. Demirbilek, S. E. Kapphan, A. B. Kutsenko and R. Pankrath, *Phys. Stat. Sol. C*, 2005, **2**, 653.

33 A. Ataei, P. McManamon, C. Bradley and R. Neurgaonkar, *Ferroelectrics*, 2023, **603**, 34.

34 S. Xia, D. Jukić, N. Wang, D. Smirnova, L. Smirnov, L. Tang, D. Song, A. Szameit, D. Leykam, J. Xu, Z. Chen and H. Buljan, *Light Sci. App.*, 2020, **9**, 147.

35 J. Li, Z. Wang, Y. Hu and J. Xu, *Laser Photonics Rev.*, 2024, **8**, 2301055.

36 R. Paszkowski, K. B. Wokulska, J. Dec and T. Łukasiewicz, *J. Cryst. Growth*, 2014, **401**, 327.

37 T. S. Chernaya, M. O. Marychev, V. A. Ivanov, N. J. Ivanov, E. V. Chuprunov, L. I. Ivleva and V. I. Simonov, *Crystallogr. Rep.*, 2007, **52**, 1056.

38 M. O Ramirez, D. Jaque, M. Montes, J. G. Solé, L. E. Bausá and L. Ivleva, *Appl. Phys. Lett.*, 2004, **84**(15), 2787.

39 M. Goulkov, T. Granzow, U. Dörfler, T. Woike, M. Imlau and R. Pankrath, *Phys. Rev. B: Condens. Matter Mater. Phys.*, 2003, **76**, 407.

40 T. Granzow, T. Woike, M. Wöhlecke, M. Imlau and W. Kleemann, *Phys. Rev. Lett.*, 2002, **89**(12), 127601.

41 K. Yao, J. D. Femi-Oyetoro, S. Yao, Y. Jiang, L. El Bouanani, D. C. Jones, P. A. Ecton, U. Philipose, M. El Bouanani and B. Rout, *2D Mater.*, 2020, **7**(1), 015024.

42 A. Castellanos-Gómez, M. Buscema, R. Molenaar, V. Singh, L. Janssen, H. S. J. van der Zant and G. A. Steele, *2D Mater.*, 2014, **1**, 011002.

43 P. Molina, M. O Ramírez and L. E. Bausá, *Adv. Funct. Mater.*, 2008, **18**, 709.

44 J. Hou, X. Wang, D. Fu, C. Ko, Y. Chen, Y. Sun, S. Lee, K. X. Wang, K. Dong, Y. Sun, S. Tongay, L. Jiao, J. Yao, K. Liu and J. Wu, *Small*, 2016, **12**, 3976.

45 S. Mouri, Y. Miyauchi and K. Matsuda, *Nano Lett.*, 2013, **13**(12), 5944.

46 J. W. Christopher, B. B. Goldberg and A. K. Swan, *Sci. Rep.*, 2017, **7**, 14062.

47 M. Buscema, G. A. Steele, H. S. J. van der Zant and A. Castellanos-Gómez, *Nano Res.*, 2014, **7**, 561.

48 K. F. Mak, K. He, C. Lee, G. H. Lee, J. Hone, T. F. Heinz and J. Shan, *Nat. Mater.*, 2013, **12**(3), 207.

49 H. J. Conley, B. Wang, J. I. Ziegler, R. F. Haglund Jr., S. T. Pantelides and K. I. Bolotin, *Nano Lett.*, 2013, **13**(8), 3626.

50 J. J. Romero, C. Aragó, J. A. Gonzalo, D. Jaque and J. G. Solé, *J. Appl. Phys.*, 2003, **93**, 3111.

51 E. L. Venturini, E. G. Spencer, P. V. Lenzo and A. A. Ballman, *J. Appl. Phys.*, 1968, **39**(1), 343.

52 K. P. O'Donnell and X. Chen, *Appl. Phys. Lett.*, 1991, **58**, 2924.

53 F. Cadiz, E. Courtade, C. Robert, G. Wang, Y. Shen, H. Cai, T. Taniguchi, K. Watanabe, H. Carrere, D. Lagarde, M. Manca, T. Amand, P. Renucci, S. Tongay, X. Marie and B. Urbaszek, *Phys. Rev. X*, 2017, **7**, 021026.